**DISCRETE ELEMENT SIMULATIONS OF VOLCANIC SPREADING: IMPLICATIONS FOR THE STRUCTURE OF OLYMPUS MONS.** J. K. Morgan[1] and P. J. McGovern[2], [1]Rice University (Dept. Earth Science, MS-126, 6100 Main Street, Houston, TX 77005; morganj@rice.edu), [2]Lunar and Planetary Institute (3600 Bay Area Blvd., Houston, TX 77058; mcgovern@lpi.usra.edu).

**Introduction:** Large basaltic volcanoes, such as Olympus Mons on Mars, and the Hawaiian volcanoes on Earth, are thought to be subject to large scale slope failure and flank collapse, which scatter landslide and avalanche debris (a.k.a., aureole deposits) about the base of the edifice [1], [2], [3], [4], [5]. Volcano growth may also be accompanied by gravitational relaxation of the edifice, referred to as volcanic spreading. This deformation is accommodated by outward flank displacement along a low-angle décollement near the base of the edifice, and thrust faults that surface at the distal edge of the volcano [6], [7]. Volcanic spreading is well documented in Hawaii [8], [9], and accounts for extensive anticlinal ridges and frontal scarps that border the submarine toes of the flanks [10], [11], [12]. A prominent scarp at the distal edge of Olympus Mons, may have a similar origin as the terrestrial flanking benches [7], [13], a hypothesis that can be tested by dynamic modeling of volcano deformation. Here, we carry out numerical simulations using the Discrete Element Method to explore the consequences of landsliding and volcanic spreading. The resulting models compare favorably to morphologic features noted on Olympus Mons, suggesting the importance of volcanic spreading in this setting.

**Background:** The enormous Olympus Mons measures 600-800 km in diameter, and reaches up to 23 km in height [13]. A steep scarp, up to 10 km high, encircles much of the lower flanks of the volcano [13]. Although the frontal scarp occurs at a remarkably constant distance from the summit, it is locally embayed, where outboard, well defined aureole lobes radiate from the base of the edifice. The association of aureole deposits and the scarp re-entrant suggests that the former derived from the collapse of the lower bench [13].

The volcanic flanks above the frontal scarp commonly exhibit concave up profiles, with the steepest slopes below the summit, and nearly horizontal slopes just behind the perimeter scarp [13]. Concentric terraces upon the upper flanks are interpreted to mark thrust faults at the downslope edges of slumps [14]. Similarly, shallow slopes above the basal scarp may reflect uplift, folding, and rotation above thrust faults at the base of edifice [6], as interpreted in Hawaii [6], [10], [11]. Continuous small scale detachment from the outer slopes of the frontal ridge would maintain the steep frontal scarp. Occasional larger slope failures may breach the lower flanks, spreading debris in front of the broken edifice to form the aureole lobes.

**Discrete Element Method:** The discrete element method (DEM) simulates an assemblage of discrete particles that interact with each other according to fundamental contact physics [15], [16]. Contact forces are summed for each particle, and an finite-difference approach is used to solve Newton's equations of motion for each particle. Several contact laws can be used, yielding a range of material rheologies. For these initial simulations, we use a Hertz-Mindlin contact theory, wherein particles respond elastically to normal forces at their boundaries, and contact shear forces are limited by interparticle sliding friction $\mu_p$ [16]. In our 2D simulations, round particles enhance particle rolling, limiting assemblage strength [16]; In order to attain realistic shear strengths, particle rotations are restricted throughout the volume. Energy is dissipated at the contacts by viscous or force damping [15].

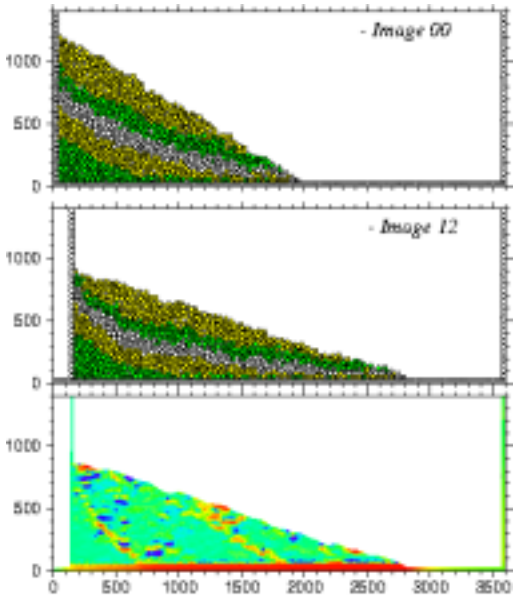


**Figure 1.** Initial and subsequent particle configurations for displacement of coherent flank. Final image shows deepe-seated landslide detachments in red.

**Numerical Simulations:** Our simple 2D experiments employ identical starting conditions: an angle-of-repose wedge of cohesive, frictional particles simulates surface lava flows and fragmental basalts banked against a vertical wall defining the mobile interior of the flank. To simulate a tectonically active volcanic

flank, the bounded side of the volcanic wedge is displaced at a steady velocity. Experiments examine the consequences of several deformation sequences, and the associated responses to variations in mechanical parameters, such as $\mu_p$, interparticle cohesion, and basal sliding friction, $\mu_b$. Here, we review two scenarios:

*Lateral flank displacement.* The bounding wall is moved at a constant rate toward the wedge, imposing a state of compression (Fig 1a). Slip occurs along the base of the wedge, transferring deformation to the toe, where thrust faults approach the surface. The oversteepened flank thins through intermittent activation of a deep seated slumps (Fig 1b and c), which sole into the deep sliding surface, and contributes to displacement of the toe. Steady displacement of the homogeneous, coherent flank produces a stable, planar slope, predicted by critical Coulomb wedge theory [18]. No frontal bench is evident (Fig 1b and c).

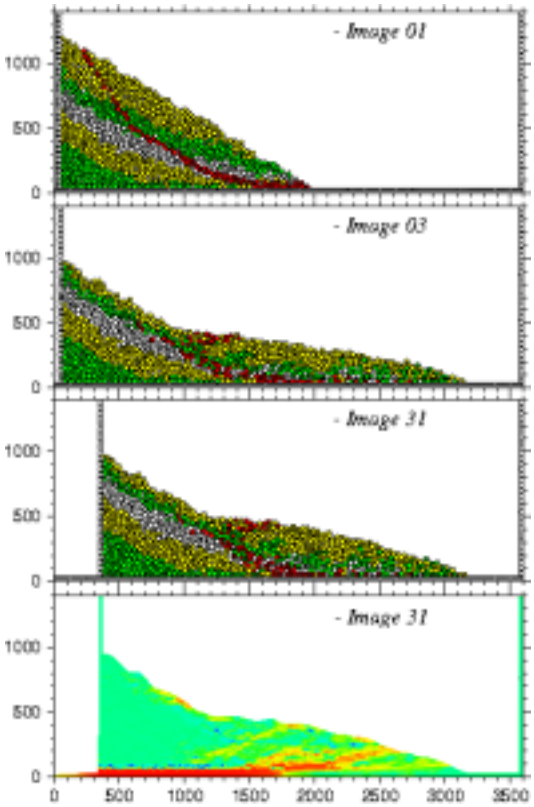


**Figure 2.** Initial and subsequent particle configurations for disintegrative slumping (red particles) and bench growth. Final image shows thrusting within bench in red.

*Sector collapse and flank displacement.* The introduction of a weak landside detachment within the wedge enables disintegrative failure of the upper flank (Fig 2a), shedding avalanche debris in front of the mobile wedge (Fig 2b). With continued displacement, the wedge plows into the flanking apron, overthrusting, uplifting, and back-rotating apron strata to build an anticlinal ridge (Fig 2c and d). The flank develops a concave up slope profile, steepest at the headwall of the failure scarp, and gentlest above the deforming debris apron. With continued thrusting, oversteepening leads to small-scale detachment of the bench outer slope, forming minor scarps (Fig 2d). An interesting secondary effect of overthrusting and uplift of the toe of the flank, is the progressive stabilization of the slopes of the upper flank, which become buttressed by the frontal bench Differing structural geometries can be produced by varying material strengths, and by preventing wholesale collapse the upper flank prior to bench growth. In all cases, the presence of loose landslide debris at the base of the sliding flank, however, leads to the growth of the frontal bench – a feature lacking in the previous simulations (Fig 1).

**Conclusions:** In summary, our simple experiments indicate that the combined effects of slope failure, debris avalanching, and lateral flank displacement, can generate the outer bench and scarp morphology observed along the perimeter of Olympus Mons. This sequence is consistent with interpretations of similar morphologic features on Kilauea and Mauna Loa volcanoes in Hawaii [11], [12]. Although our model conditions are very simplified, they demonstrate the importance of the dynamic interplay between landsliding and volcanic spreading, The Mauna Loa aureole deposits, which hint of past slope failures, may also have been necessary ingredients in the formation of perimeter scarps, which in turn have stabilized the volcanic edifice. The important similarities between Olympus Mons and better studied terrestrial examples, such as Hawaii, suggest that we may productively expand this analogy to clarify the dynamic evolution of Olympus Mons volcano and its aureole deposits.

**References:** [1] Holcomb, R. T., and Searle, R.C. (1991) *Marine Geotech., 10,* 19. [2] Moore, J.G. et al. (1989) *JGR, 94,* 17,465. [3] Lopes, R.M. et al. (1980) *Moon Planets, 22,* 221. [4] Lopes, R.M. et al. (1982) *JGR, 87,* 9917. [5] McGovern, P.J., and Solomon, S.C. (1993) *JGR, 98,* 23,553. [6] Borgia, A. et al. (1990) *JGR, 95,* 14,357. [7] Borgia, A. et al. (2000) *Ann. Rev. Earth Planet. Sci.,* 28,539. [8] Delaney, P.T. et al. (1998), *JGR, 103,* 18,003. [9] Owen. S. et al., (2000) *JGR, 105,* 18,983. [10] Denlinger, R.P., and Okubo, P. (1995) *JGR, 100,* 24,499. [11] Morgan, J.K. et al. (2000) *Geology, 28,* 667. [12] Morgan, J.K., and Clague, D.A. (2003) *Geology, in press.* [13] McGovern, P.J., et al. (2003) *this volume*. [14] Thomas, P.J. et al. (1990) *JGR, 95,* 14, 345. [15] Cundall, P.A., and Strack, O.D.L. (1979) *Geotechnique, 29,* 47. [16] Morgan, J.K., and Boettcher, M.S. (1999) *JGR, 104,* 2703. [18] Davis, D. et al. (1983) *JGR, 88,* 1153.